

Time-Dependent Erosion of Ion Optics

Richard E. Wirz¹, John R. Anderson², Ira Katz³, and Dan M. Goebel⁴
Jet Propulsion Laboratory, California Institute of Technology, Pasadena, CA, 91001

The accurate prediction of thruster life requires time-dependent erosion estimates for the ion optics assembly. Such information is critical to end-of-life mechanisms such as electron backstreaming. CEX2D was recently modified to handle time-dependent erosion, double ions, and multiple throttle conditions in a single run. The modified code is called “CEX2D-t”. Comparisons of CEX2D-t results with LDT and ELT post-tests results show good agreement for both screen and accel grid erosion including important erosion features such as chamfering of the downstream end of the accel grid and reduced rate of accel grid aperture enlargement with time.

Nomenclature

e	=	electron charge
j_c	=	ion current density calculated by code
j^+	=	current density of singly-charged ions
j^{++}	=	current density of doubly-charged ions
KE	=	kinetic energy
n	=	number density
\dot{n}	=	generation rate
q	=	space charge density
v	=	velocity
Y	=	sputter yield
γ	=	double ion ratio j^{++}/j^+
σ	=	collision cross-section

I. Introduction

ION optics erosion is one of the most critical life-limiting mechanism for ion thrusters. Significant erosion of the ion optics grids was observed during the long duration test (LDT) and the extended life test (ELT) of the NSTAR thruster [1,2]. This erosion resulted in excessive electron backstreaming at the highest throttle condition for the NSTAR thruster during the ELT. Grid erosion models shows that strict cylindrical erosion of the accel grid holes does not explain the increase in electron backstreaming [2]. It is apparent that chamfering of the upstream end of the accel grid holes contributed to the high rates of EBS later in the thruster’s life. To capture the effects of this hole chamfering and other grid erosion phenomena, a self-consistent method for estimating the time dependent grid erosion is needed. The ultimate goal of this model is to work with the self-consistent electron backstreaming model discussed in reference [3] and other models to accurately predict long-term thruster performance and end-of-life (EOL) conditions. The objective of this effort is to demonstrate a 2D model that accurately treats the time-dependent erosion of ion thruster optics.

¹ Senior Engineer, Electric Propulsion Group, 4800 Oak Grove, M-S 125-109.

² Senior Engineer, Electric Propulsion.

³ Group Supervisor, Electric Propulsion Group.

⁴ Senior Research Scientist, Propulsion and Materials Engineering Section.

II. Formulation and Inputs

A technique for estimating the time-dependent erosion of the ion optics was developed using the CEX2D ion optics code. For clarity, this new version of the code that performs time-dependent grid erosion will be referred to as “CEX2D-t”. Previous to this study, CEX2D provided erosion rates for a predefined grid shape comprised of simple geometric shapes. The code was modified to use the erosion rate information to reduce the mass represented by the nodes defining the grid until the node’s mass is reduced to zero. Once a node’s mass is eliminated, the geometry is modified accordingly, the ion optics code is then re-run to redefine the local potentials in the computational domain to determine the new beamlet characteristics in light of the new geometry. The new beamlet characteristics are then used to recompute the grid erosion rates until another node is eliminated. The grid geometry and remaining mass at each node is stored for each iteration. This process is repeated until a predefined thruster operation time is reached. The user may define various operating condition for a series of thruster operating times to demonstrate throttled operation such as demonstrated in the ELT. As discussed below, the effects of double ions on space charge and sputter yield were added to CEX2D-t as well.

A. Double ions formulation

The CEX2D-t code assumes that the plasma consists entirely of singly charged xenon ions. However, the results can be rigorously scaled to a double ion current ratio, γ , to determine the corrected sputter yield and charge density values from plasma bombardment of the upstream face of the screen grids and direct impingement of other grid surfaces. We rely on the fact that in a steady state potential without magnetic fields, single ions and double ions follow the same trajectories, just that double ions move faster. The current density found by the code is the sum of the single and double ion (assuming no other ion species) such that

$$j^c = j^+ + j^{++} = j^+ (1 + \gamma) \quad (1)$$

Therefore,

$$\begin{aligned} j^+ &= \frac{1}{1 + \gamma} j^c \\ j^{++} &= \frac{\gamma}{1 + \gamma} j^c \end{aligned} \quad (2)$$

For sputtering from direct impingement from beam ions we need to determine the fluxes of singly and doubly ionized particles to the surface. For this, the current densities are related to the ion generation rates by

$$\begin{aligned} j^+ &= e\dot{n}^+ \\ j^{++} &= 2e\dot{n}^{++} \end{aligned} \quad (3)$$

Such that

$$\begin{aligned} \dot{n}^+ &= \frac{1}{(1 + \gamma)} \frac{j^c}{e} \\ \dot{n}^{++} &= \frac{\gamma}{(1 + \gamma)} \frac{j^c}{2e} \end{aligned} \quad (4)$$

Therefore, the sputter yield due to impact of beamlet and discharge ions with grid surfaces, including the effects of double ions, is

$$Y_{dc} = Y(KE^+) \dot{n}^+ + Y(KE^{++}) \dot{n}^{++} \quad (5)$$

Combining the above relations yields an expression for the sputter yield from discharge chamber ions, Y_{dc} , in terms of the current density provided by the code and the double-to-single ion current ratio

$$Y_{dc} = \frac{j^c}{e(1+\gamma)} \left[Y(KE^+) + Y(KE^{++}) \frac{\gamma}{2} \right] \quad (6)$$

The change in sputter yield due to doubly-charged charge-exchange ions is computed by considering the xenon charge-exchange cross-sections given in reference [4]. The code determines the current of CEX ions generated in a region of beamlet from

$$j_{CEX}^c = j_c n_o \sigma_{CEX^+}^{Xe^+} (KE^+) \quad (7)$$

where $\sigma_{CEX^+}^{Xe^+}$ is the collision cross-sections for singly-charged CEX ions created by singly-charged beamlet ions. To correct this expression for doubly-charged ions we consider that the actual generation rates for singly- and doubly-charged ions are given by

$$\begin{aligned} e\dot{n}_{CEX}^+ &= n_o j^+ \sigma_{CEX^+}^{Xe^+} (KE^+) \\ 2e\dot{n}_{CEX}^{++} &= n_o j^{++} \sigma_{CEX^{++}}^{Xe^{2+}} (KE^{++}) \end{aligned} \quad (8)$$

where $\sigma_{CEX^{++}}^{Xe^{2+}}$ is the collision cross-sections for doubly-charged CEX ions created by doubly-charged beamlet ions. The cross-sections given in reference [4] show that the CEX generation mechanisms from the preceding equations dominate CEX production for ion thruster plumes. For example, the cross-section for singly-charge CEX ions created by doubly-charged beamlet ions, $\sigma_{CEX^+}^{Xe^{2+}}$, is over an order of magnitude smaller than $\sigma_{CEX^+}^{Xe^+}$; which results in a negligible effect for $\gamma < 1$. Combining the above equations gives

$$\begin{aligned} \dot{n}_{CEX}^+ &= \frac{1}{1+\gamma} \frac{j_{CEX}^c}{e} \\ \dot{n}_{CEX}^{++} &= \frac{\gamma}{1+\gamma} \frac{j_{CEX}^c}{2e} \frac{\sigma_{CEX^{++}}^{Xe^{2+}} (KE^{++})}{\sigma_{CEX^+}^{Xe^+} (KE^+)} \end{aligned} \quad (9)$$

The sputter yield for charge exchange ions is found from

$$Y_{CEX} = Y(KE_{CEX}^+) \dot{n}_{CEX}^+ + Y(KE_{CEX}^{++}) \dot{n}_{CEX}^{++} \quad (10)$$

Therefore, solving for the charge exchange sputter yield gives

$$Y_{CEX} = \frac{j_{CEX}^c}{e(1+\gamma)} \left[Y(KE_{CEX}^+) + Y(KE_{CEX}^{++}) \frac{\gamma}{2} \frac{\sigma_{CEX^{++}}^{Xe^{2+}} (KE^{++})}{\sigma_{CEX^+}^{Xe^+} (KE^+)} \right] \quad (11)$$

The space charge density is computed by adding the charge densities of singly- and doubly-charged ions for a given double ion current ratio. Since the code uses singly-charged ions for its initial charge density the charge density due to singly-charged ions, in terms of the charge density calculated by the code, q_c , is

$$q^+ = \frac{1}{(1+\gamma)} \frac{j^c}{v^+} = \frac{1}{1+\gamma} q^c \quad (12)$$

and, similarly, the charge density due to doubly-charged ions is

$$q^{++} = \frac{\gamma}{(1+\gamma)} \frac{j^c}{v^{++}} = \frac{\gamma/\sqrt{2}}{1+\gamma} q^c \quad (13)$$

Summing these charge densities gives the total charge density corrected for double ions

$$q = \frac{1+\gamma/\sqrt{2}}{1+\gamma} q^c \quad (14)$$

B. Sputter Yield

The NSTAR ion thruster uses xenon propellant and molybdenum ion optics grids. The sputter yields for xenon on molybdenum for normal incidence used in this effort were taken from references [5] and [6]. Yield curves were fitted to Rosenberg's data for $\text{Xe}^+ \rightarrow \text{Mo}$ incidence energies above 140 eV while the Doener's spectroscopic yield data was used for incidence energies below 60 eV. Rosenberg's and Doener's data were linearly averaged between for normal incidence between 60 and 140 eV. The technique for accounting for off-normal incidence is given in reference [7].

C. Thruster and Plasma Parameters

Post-test analysis of the NSTAR thrusters at the conclusion of the LDT and ELT tests showed that the center region of the grids experienced the most erosion and accel grid aperture enlargement, features which lead to increased electron backstreaming [3]. To simulate worst-case erosion, the code was run at center beamlet conditions for the full duration of the ELT using the thruster operating conditions shown in Table 1. The beamlet currents used in the analysis are shown in Figure 1; these beamlet current profiles were calculated from LDT and ELT Faraday probe traces using the technique discussed in reference [2]. The neutral densities for TH12 and TH15 were taken as the average of the neutral from the exit plane neutral profiles in reference [8] and were scaled to the discharge flows rates for TH0, TH5, and TH8. The potential for the downstream beam plasma, ϕ_{bp} , and electron temperature, T_e were taken as 15 V and 1.8 eV, respectively, as discussed in [2]. The upstream electron temperature used was 5 eV. The centerline double ion content estimates were taken from ExB data from the ELT and Dawn pre-flight tests. The grid dimensions have been previously been reported in several papers, including reference [9].

The nominal grid gap chosen for this analysis was the 0.30 mm spacing measured for TH15 in reference [refSoulasexp] (this assumes an initial cold grid gap of 0.66 mm and a lessening of the grid gap by 0.36 mm). However, the uncertainty in the change in grid gap measurement was ± 0.073 mm and the uncertainty in the measured cold grid gap is approximately ± 0.015 mm. Reference [refSoulasexp] also showed that the grid gap change is likely closer to -0.02 mm for TH0 (-0.35 for TH8). Post-test analysis for the LDT and ELT showed that the cold grid gap had changed approximately -0.08 mm and -0.20 mm, respectively. From these data it is clear that the grid gap measurement is highly uncertain and the grid gap value for a given throttle level may change during the test. At this time, the code does not allow for the grid gap to change during a given run; therefore, a range of constant grid gaps were used on several runs to assess erosion sensitivity to grid gap choice. The results from these runs are shown in the following section.

III. Analysis and Results

A simple parametric analysis of the above equations provides an indication of the importance of considering double ions for grid erosion analysis. This analysis is not entirely self-consistent, but it provides a means to interpret the erosion estimates made by CEX2D-t. The relative sputter yield for the impact of discharge ions of the upstream surface (using Y_{dc}) was analyzed assuming discharge ion hit the screen grid with energy approximately equal to the discharge voltage plus the energy from the Bohm sheath assumption ($Te/2$); therefore an energy of approximately

27.5 V was used for single ions. The sensitivity analysis for sputter yield due to charge exchange ions on the accel grid (using Y_{CEX}) by assuming the singly-charged ion energy is the beam plasma potential minus the accel grid potential (i.e., for single ions the nominal case gives $\phi_{bp} - V_a = 15 + 180 = 195$ V; worst-case gives $\phi_{bp} - V_a = 15 + 260 = 275$ V). A basic diagram of the grids and grid erosion mechanisms is shown in Figure 1. The results of this simple parametric analysis are shown in Figure 2. These results show that an increased double ion ratio (which can be as high as 0.3 for NSTAR on centerline) significantly increases the direct sputter yield for the screen grid. The accel grid erosion due to charge exchange ions decreases for increasing double ion content due to the fact that the effective number of ions is reduced by a factor of two and the yield at double ion energy is less than twice that for single ions at the energies of interest; in addition, at these energies the ratio of the collision cross-sections for doubly- to singly-charged CEX ions is less than 0.5. The results also show that increased double ion content reduces charge density modestly, which is clear from the resulting equation from the formulation above.

To provide a comparison with the computational results, a cross-section of the center hole on the accel grid for the LDT is shown in Figure 3 at the conclusion of the 8200 hour test. A cross-section of the center-hole accel grid at the conclusion of the 30,352 hr ELT is shown in Figure 4. These cross-sections will be used to compare to the accel grid erosion patterns determined by the code. For the screen grid erosion we will simply estimate a chamfered shape and screen grid thickness change from the LDT and ELT test data as shown in Figure 5. During the LDT the upstream side of the screen grid chamfered at a depth of up to 40 μm and a width of up to 80 μm at the center hole, with an overall thickness reduction of up to ~ 20 μm . The ELT experienced similar chamfering of the screen grid and over 80 μm of the overall surface on upstream side of the screen grid was eroded away by the end of the test.

Time-dependent screen and accel grid erosion profiles were determined for the NSTAR LDT and ELT test using CEX2D-t and the parameters discussed above and shown in Table 1. Center hole erosion for the LDT was simulated by running the TH15 condition from Test Segment “2” of the ELT from 0 to 8200 hours at a slightly higher beamlet current density to match the slightly higher centerline beam current as shown in Figure 1. The beginning-of-life grid geometry and mesh are shown in Figure 5. The erosion estimate by CEX2D-t for the 8200 hr LDT, shown in Figure 6, compares well to experimental profiles derived from LDT data. The disagreement related to erosion of the downstream end of the accel grid (commonly referred to as “pits & grooves” erosion) is expected since the erosion in this region near the radial maximum of the domain is better treated by a 3D code, such as CEX3D, due to the inherent 3D nature of this region for the hexagonal geometry of the gridlet, as described in [10]. The code nearly predicts the magnitude of upstream screen grid erosion but does not demonstrate the chamfering of the screen grid as observed in post-test analyses; this may also be resolved by a 3D treatment. Another consideration is to modify the velocity with which the ions are introduced from the upstream surface of the computational domain. At this time, the ions enter the domain with the Bohm velocity, which may be too high for the ions to be properly affected by potentials caused by the beamlet sheath.

The results for the predicted erosion profiles at the end of the seven test segments of the ELT are shown in Figure 7. The expired times do not match the ELT exactly since the code time steps are dictated by node losses; this inaccuracy is most notable for the end of Test Segment 5 where TH0 progresses for over 1400 hrs beyond the prescribed end time. These data show the “cusp erosion” \rightarrow “cylindrical erosion” \rightarrow “chamfer erosion” behavior predicted by Brophy [2], the approximate timeline of which is shown later in Figure 10. To examine the influence of double ions, the same parameters for the ELT were used except without double ions (i.e., $\gamma = 0$). The results of this computational sensitivity analysis, shown in Figure 8, agree with the parametric analysis in that the doubles will greatly augment upstream screen erosion and will have little effect on the accel grid erosion. A similar sensitivity was performed with grid spacing, using constant grid spacings of 200 and 400 μm to compare with the nominal 300 μm spacing. The erosion profiles for the 200 μm spacing from Figure 9 show that the accel grid erosion is very similar to the nominal case. The slightly lower screen erosion is expected since the smaller 200 μm spacing increases the ion transparency of the grids, thus reducing the upstream plasma density requirements and reducing the ion bombardment rate on the upstream screen grid surface. Figure 10 shows the estimated accel hole diameter determined by the code for constant grid gaps of 200, 300, and 400 μm , compared against data measured from the ELT. The results for all cases compare well with the experimental data; however aperture diameters later in the test are smaller since the model is not predicting the slight upstream chamfering observed in the test. This upstream chamfering is observed for simulations performed for the properties of gridlets at a grid radius of 7 cm but additional analysis is needed to determine what is causing the upstream chamfering.

IV. Conclusion

This effort represents a significant step towards using modeling to aid in the prediction of ion thruster performance and life for long duration missions. The code predicts the major features of grid erosion observed in the LDT and ELT tests. Double ions greatly increase the screen grid erosion and mitigate the effects of accel grid erosion due to CEX ions. The code currently uses only one grid space for an entire run. Results herein show that useful results can be obtained with this limitation; however, the code will benefit greatly from adding the ability to change grid gap as the run progresses which should improve the prediction of life-limiting mechanisms. The code will also benefit with increased knowledge of inputs (e.g., local double ion content, neutral density, sputter yields, etc.) and experimental erosion measurements (e.g., grid geometry as a function of time) since there is non-negligible uncertainty in many of the parameters used herein, though such an improvement is not necessary for this initial code validation effort. This 2D treatment is sufficient to describe general features; however, a 3D treatment is necessary to capture, accurately, effects near the radial maximum of the axially symmetric computational boundary, such as pits and grooves erosion of the accel grid and chamfering of the upstream surface of the accel grid. Additional efforts may also include redeposition sputtered grid material, as well as, redeposition of sputtered facility surfaces for long duration test validation efforts.

Appendix

Table 1. Input Parameters for Simulation of ELT

Test Segment	Throttle Level	J_b (mA)	Pwr (kW)	V_b	γ (ctr)	V_a	n_o (local)	End Time (khr)
1	TH12	1.49	1.96	1100	0.291	-180	7.30E+17	0.447
2	TH15	1.76	2.33	1100	0.297	-180	7.50E+17	4.693
3	TH8	1.1	1.46	1100	0.238	-180	3.88E+17	10.451
4	TH15	1.76	2.33	1100	0.227	-260	5.67E+17	15.617
5	TH0	0.51	0.52	650	0.061	-150	2.08E+17	21.306
6	TH15	1.76	2.33	1100	0.262	-260	5.81E+17	25.706
7	TH5	0.81	1.12	1100	0.197	-250	2.22E+17	30.352

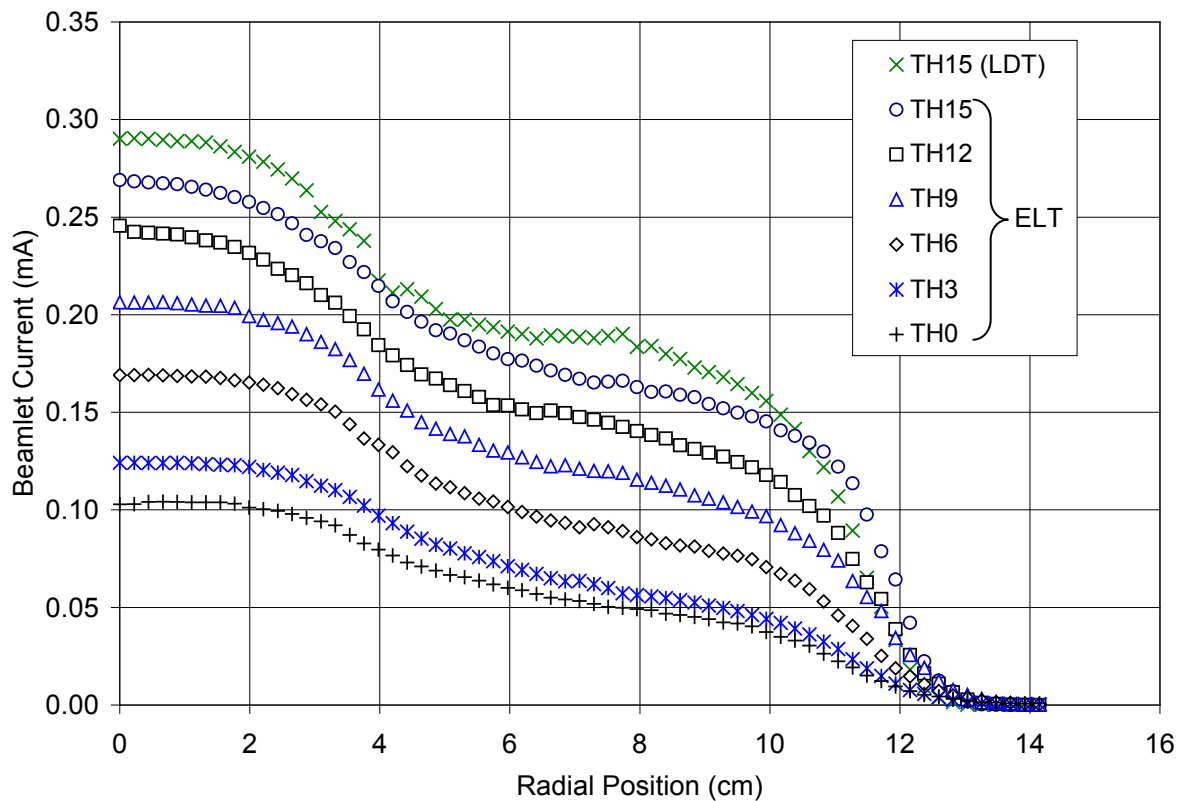


Figure 1. Beamlet current vs. radial position for LDT at TH15 and ELT for various throttle conditions.

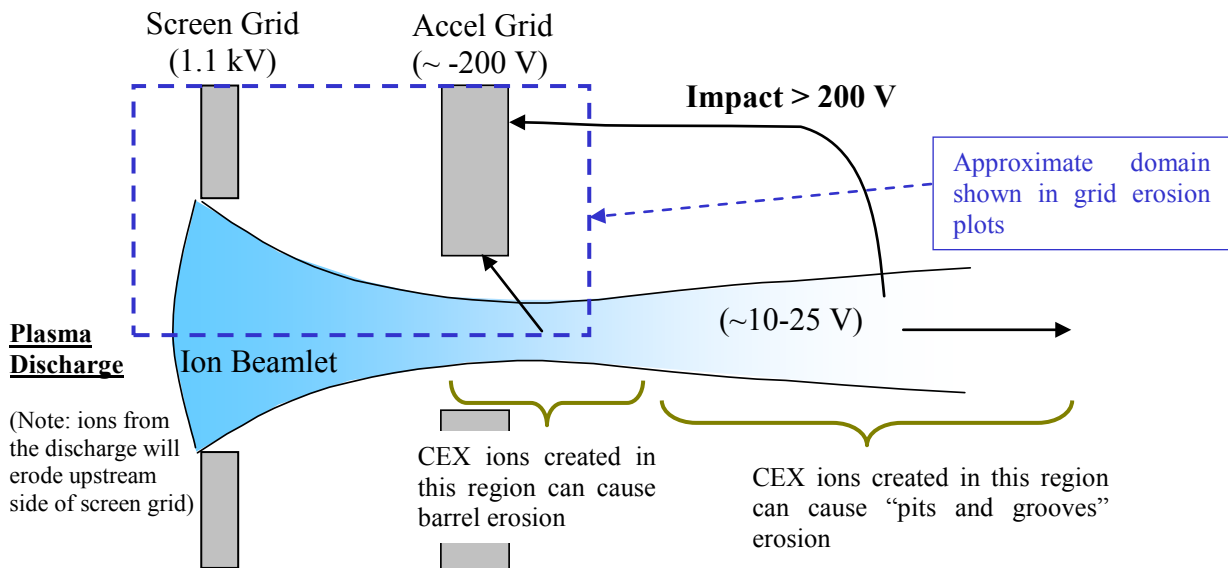


Figure 2. Diagram of CEX erosion mechanisms for a single beamlet. Also shown is the portion the of computational domain used to show CEX2D-t grid erosion estimates in later figures (note: entire computational domain extends 5 cm downstream).

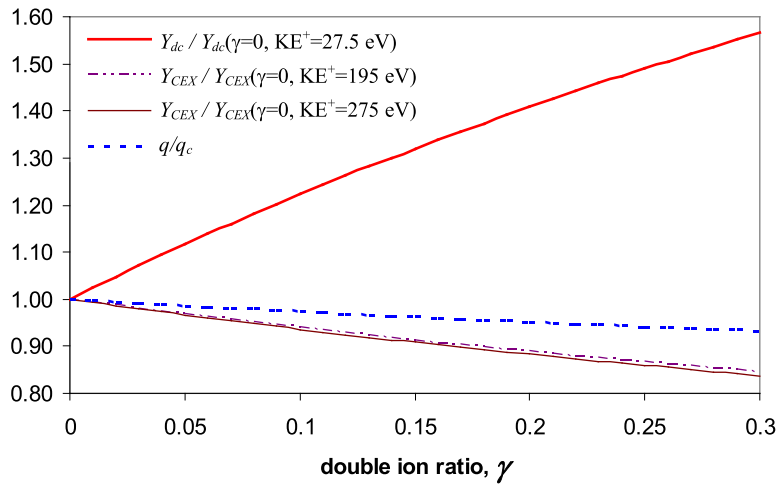


Figure 3. Sensitivity analysis of sputter yield and charge density vs. double ion ratio.

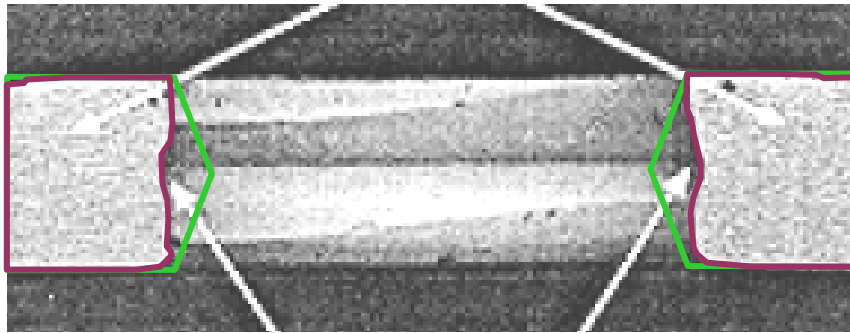


Figure 4. Center-hole accel grid cross-section after 8200 hour LDT at TH15. Approximate beginning-of-life (BOL) grid geometry is shown in solid green. Comparison of hole wall topography shows that the erosion is very nearly symmetric about gridlet axis. Original image from reference [refLDT].

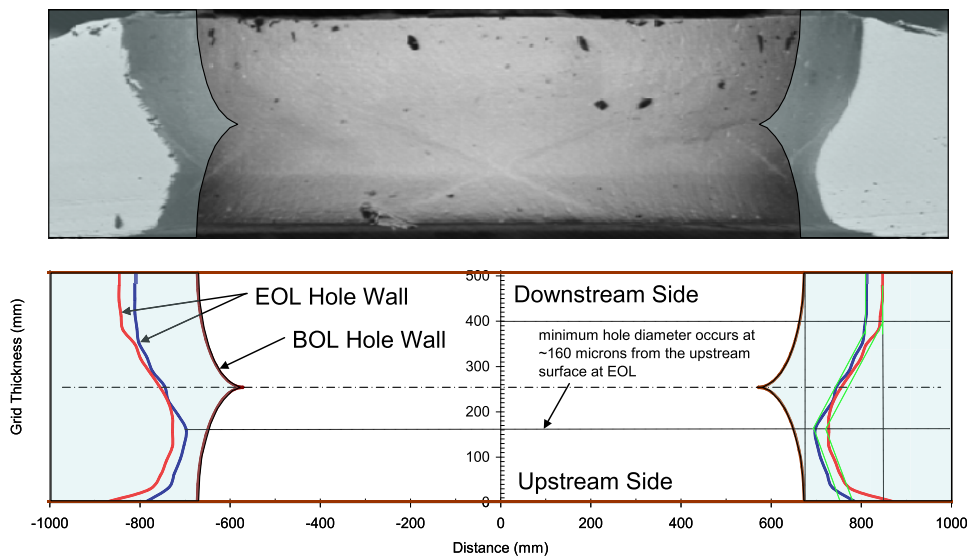


Figure 5. Cross-section of center hole accel grid for ELT compared with approximate BOL geometry. Erosion pattern shows some departure from axisymmetry. Figure taken from reference [refBrophyEBS].

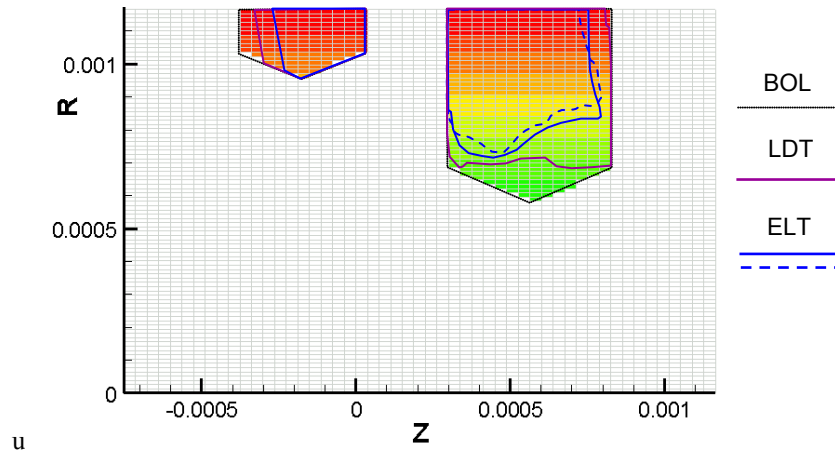


Figure 6. Beginning-of-Life (BOL) grid geometry at start of simulation. Computational in grid near-field is shown; however, mesh extends 5 cm downstream to include downstream CEX ions that contribute to erosion.

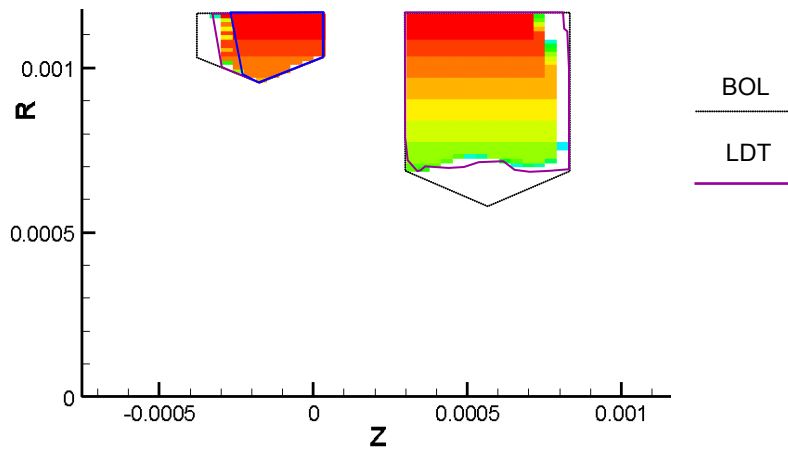


Figure 7. LDT erosion estimate after 8200 hours, compared with experimental profiles.

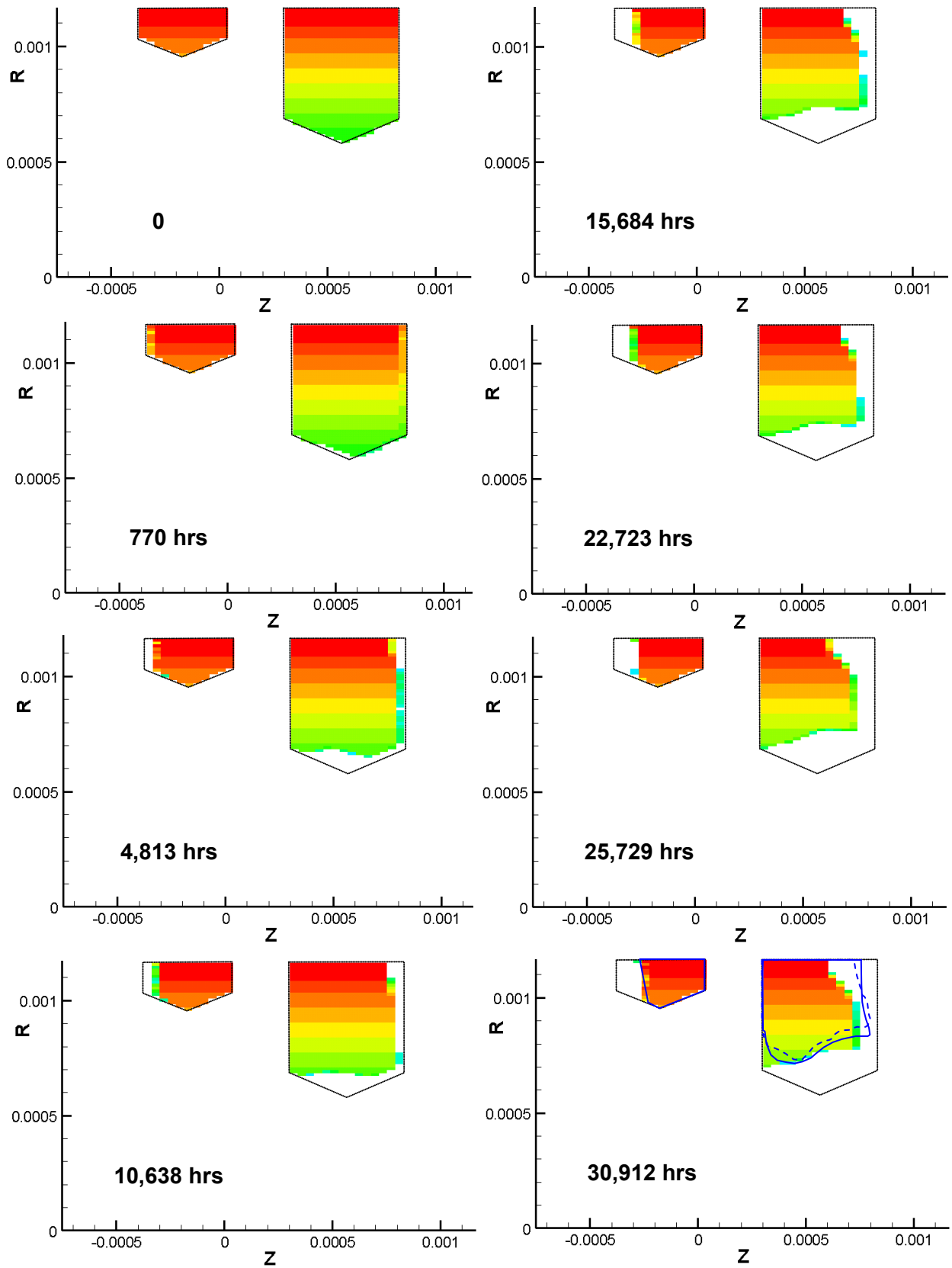


Figure 8. Progressive time-dependent erosion estimate for ELT using CEX2D-t.

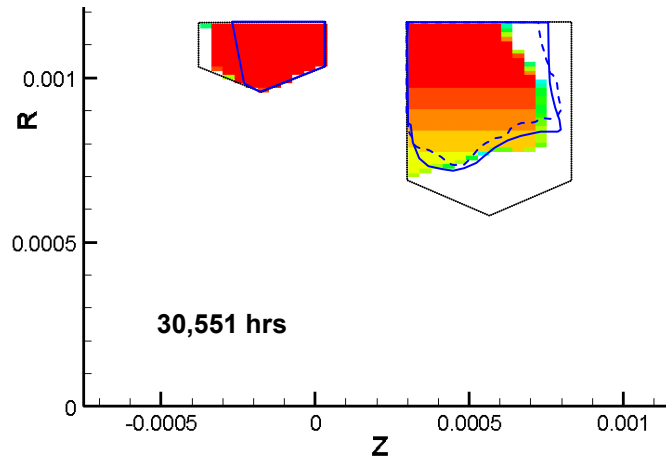


Figure 9. Final erosion profile for ELT without double ions, $\gamma = 0$ (grid gap = 300 μm).

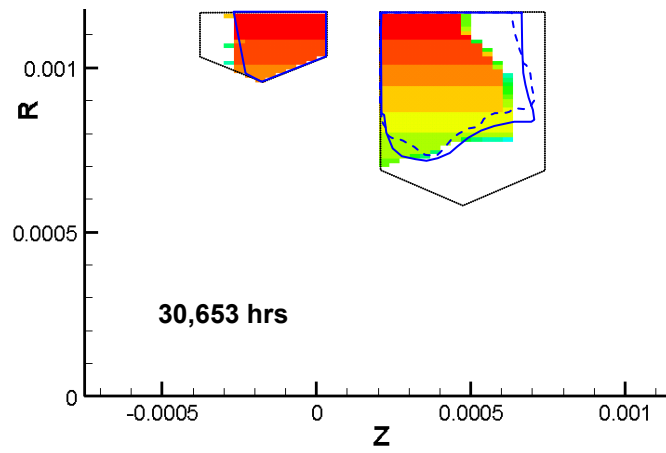


Figure 10. Final erosion profile for ELT using constant grid gap of 200 μm .

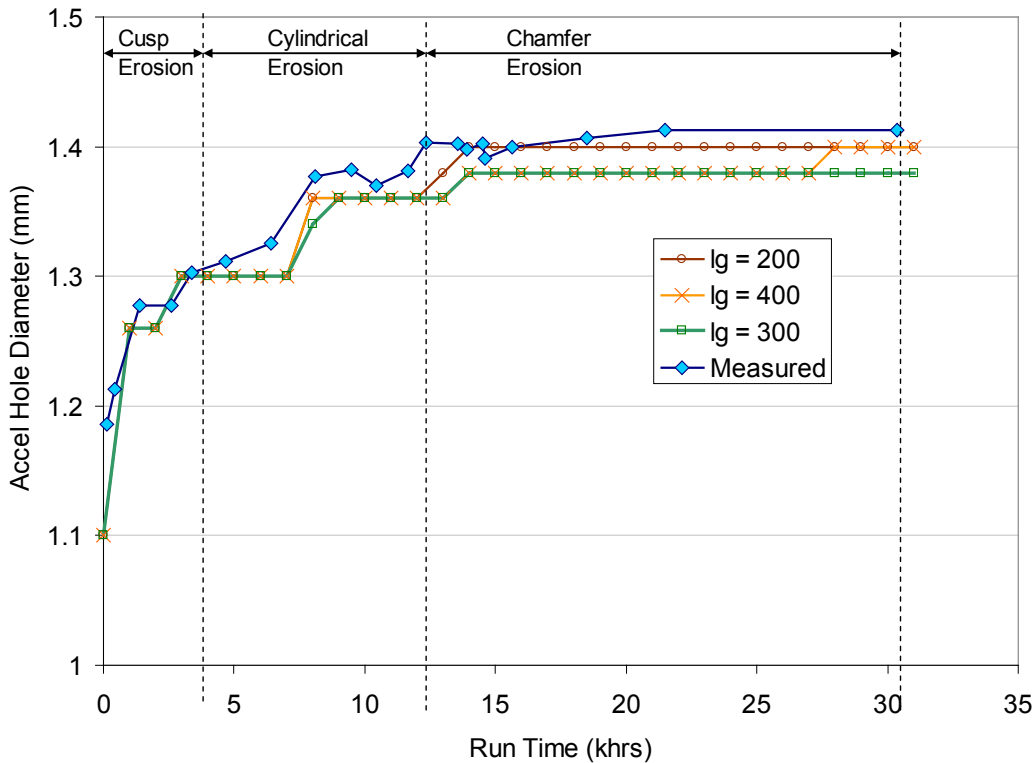


Figure 11. Accel grid center hole diameter vs. time simulations of ELT using CEX2Dt. Results are shown for constant grid gaps of 200, 300, and 400 microns.

Acknowledgments

The research described in this paper was carried out by the Jet Propulsion Laboratory, California Institute of Technology, under contract with the National Aeronautics and Space Administration..

References

- ¹ Polk J. E., Anderson J. R., Brophy J. R., "An Overview of the Results from an 8200 Hour Wear Test of the NSTAR Ion Thruster," AIAA 99-2446
- ² Brophy J.R., "Propellant Throughput Capability of the Dawn Ion Thrusters," IEPC-2007-279
- ³ Wirz R., Katz I., Goebel D., Anderson J. R., "Electron Backstreaming Determination for Ion Thrusters," AIAA-2008-4732
- ⁴ Miller J. S., et al, "Xenon charge exchange cross-sections for electrostatic thruster models," *Journal of Applied Physics*, Vol. 91, No. 3, 2002, pp. 984 – 991.
- ⁵ Doerner, R. P., Whyte, D. G., and Goebel, D. M., "Sputtering Yield Measurements During Low Energy Xenon Plasma Bombardment," *Journal of Applied Physics*, Vol. 93, No. 9, May 2003, pp. 5816-5823.
- ⁶ Rosenberg, D., and Wehner, G. K., "Sputtering Yields at Very Low Energy He⁺, Kr⁺, and Xe⁺ Ion Bombardment," *Journal of Applied Physics*, Vol. 33, No. 7, 1962, pg. 1824.
- ⁷ Brophy J. R., Katz I., Polk J., Anderson J. R., "Numerical Simulations of Ion Thruster Accelerator Grid Erosion," AIAA 2002-4261
- ⁸ Wirz R., "Discharge Plasma Processes of Ring-Cusp Ion Thrusters," Ph.D. Dissertation, Aeronautics, Caltech, Pasadena, CA, 2005, <http://etd.caltech.edu/etd/available/etd-05232005-162628/>.
- ⁹ M.J. Patterson, et al, "NASA 30 cm ion thruster development status," AIAA-94-2849
- ¹⁰ Anderson J. R., Katz I., Goebel D., "Numerical Simulations of Two-Grid Ion Optics Using a 3D Code," AIAA 2004-3782